

# Particle Filter Networks with Application to Visual Localization

Peter Karkus<sup>1,2</sup>    David Hsu<sup>1,2</sup>    Wee Sun Lee<sup>2</sup>

<sup>1</sup>NUS Graduate School for Integrative Sciences and Engineering

<sup>2</sup>School of Computing

National University of Singapore

{karkus, dyhsu, leews}@comp.nus.edu.sg

**Abstract:** Particle filtering is a powerful method for sequential state estimation and is extensively used in many domains, including robot localization, visual tracking, etc. To apply particle filters in practice, a main challenge is to construct an effective probabilistic system model, especially when the system exhibits complex dynamic behavior or processes rich sensor information from, e.g., visual cameras. This paper introduces the Particle Filter Network (PF-Net), which captures both a system model and the particle filter algorithm in a single neural network. This unified network representation enables end-to-end model learning, which trains the model in the context of a specific algorithm, resulting in improved performance, compared with conventional model-learning methods. We apply PF-Net to visual robot localization. The robot must localize in rich 3-D environments, using only a schematic 2-D floor map. In preliminary experiments, PF-Net consistently outperformed alternative learning architectures, as well as conventional model-based localization methods. PF-Net learns effective models that generalize to new, unseen environments. It can also incorporate semantic labels on the floor map.

**Keywords:** state estimation, deep neural network, end-to-end learning, localization

## 1 Introduction

Particle filters, also known as sequential Monte-Carlo methods, build on the powerful idea of representing an arbitrary probability distribution by a set of particles, i.e., weighted samples from the distribution [1]. They are extensively used in robotics [2, 3, 4], as well as in computer vision, physics and econometrics [5, 6, 7, 8, 9]. Particle representations are critical in robotic tasks: localization [2], SLAM [4], and planning under partial observability [10]. A major barrier of applying particle filtering in practice is to construct probabilistic system models or learn them from data [11, 12, 13]. Consider robot localization with an onboard camera. The observation model is a probability distribution over the set of all possible camera images, conditioned on a continuous state and a map. Learning such a model is challenging, because of the enormous space and lack of suitably labeled data.

An emerging line of recent work circumvents the difficulty of traditional model learning by integrating algorithmic structures into deep neural networks and then learning models end-to-end [14, 15, 16, 17, 18, 19, 20]. Sequential state estimation has been addressed in the form of Kalman filters [15] and histogram filters [16, 17, 21]. They represent the probability distribution by a Gaussian and a discrete histogram, respectively, and thus they are unsuitable for many robotic problems, e.g., localization.

We introduce the Particle Filter Network (PF-Net), a recurrent neural network (RNN) with algorithmic priors for probabilistic state estimation (Fig. 1a). PF-Net encodes learnable probabilistic transition and observation models, together with the particle filter algorithm, in a single neural network. PF-Net addresses the key challenges of learning complex probabilistic models. Neural networks can represent complex functions over a large space, e.g. images. The particle filter algorithm, encoded in the same network, allows learning the models end-to-end. Instead of constructing a full conditional distribution, end-to-end models may learn only the features relevant to state estimation, without supervision on the model components. Unlike Kalman filters and histogram filters, PF-Net can efficiently approximate arbitrary, continuous distributions, making them applicable to a wide range of tasks. In this paper

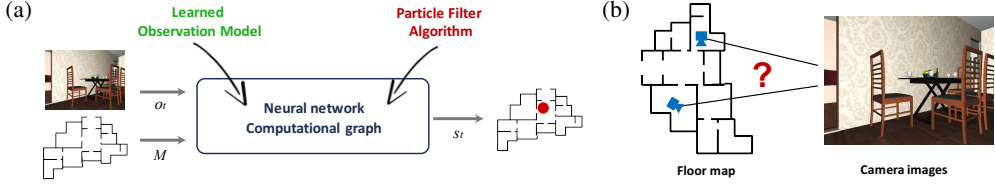


Figure 1: (a) PF-Net encodes both a probabilistic system model and the particle filter algorithm in a single, unified neural network. It trains the model in the context of a specific algorithm, resulting in improved performance. (b) Robot visual localization in a rich 3-D environment, using only a schematic 2-D floor map. The robot must match visual features with the map geometry, while ignoring objects not on the map, e.g., furniture.

we restrict our investigation to visual localization in previously unseen environments given a 2-D map (Fig. 1b). The task exhibits key challenges of sequential state estimation from ambiguous, partial observations, and it is of great interest for mobile robot applications.

A robot navigates in a previously unseen environment, while it does not know its exact location. The task is to periodically estimate the location given a 2-D floor map and the history of observations from onboard sensors. Particle filtering, i.e., Monte-Carlo localization, is the standard approach for laser sensors [2]. Here we apply PF-nets to localization with visual sensors, e.g., a camera. The difficulty now is the probabilistic observation model. It must match the crude 2-D geometry from the map, with rich, 3-D visual features from camera images, which also show objects not on the map, e.g., furniture. A model-based approach would need to construct a conditional distribution of images showing environments with different layouts, configurations of different furniture, etc. In contrast, PF-net model are trained end-to-end, and thus they only learn features relevant for localization.

This paper makes two contributions. First, we encode the particle filter algorithm in a neural network to learn models for state estimation end-to-end. Second, we apply PF-net to the robot visual localization task and present a network architecture for matching features from camera images of a rich 3-D world with a 2-D floor map. Preliminary results on the House3D data set [22] show that PF-nets are effective for visual localization in new environments, populated with furniture. Through end-to-end training, PF-nets can learn better models than conventional model-based methods; fuse information from RGB and depth cameras; and use semantic maps, i.e., labels for doors and rooms.

## 2 Related work

Integrating algorithmic priors with deep neural networks has been gaining attention recently. The idea was applied to decision making in the context of value iteration in Markov decision processes [14], searching in graphs [18, 19, 23], path integral optimal control [24], quadratic program optimization [20, 25], and planning under partial observability [17, 21]. Probabilistic state estimation was addressed by Haarnoja et al. who encoded Kalman filters in a neural network [15]. The probability distributions are limited to unimodal Gaussian. Jonschkowski and Brock introduced end-to-end histogram filters [16], and such filters were used by Karkus et al. [17] and Shankar et al. [21] for policy learning under partial observability. Histogram filters use a discrete representation and thus they are inherently limited to small state spaces. In contrast, we use particle filters that can efficiently approximate an unrestricted class of distributions over large, continuous spaces.

Concurrent to our work, Jonschkowski et al. have been independently working on the related idea of differentiable particle filtering [26]. Despite the similarity, we would like to highlight two important differences. First, we propose a differentiable approximation of the resampling operation, an important issue not addressed in the concurrent work [26]. Second, we apply PF-nets to visual localization in previously *unseen* environments, after learning. While the concurrent work also deals with localization, it does so in a fixed environment. Our approach addresses the challenge of matching features from both a map and camera images. Further, we learn to handle furniture not indicated on the map, and to incorporate information from multiple sensors and semantic maps.

Neural networks have been used with particle filtering in the context of variational learning, where they parameterize a family of distributions [27, 28, 29, 30]. Unlike PF-nets, they explicitly represent a generative distribution of observations, making them unsuitable, e.g., for camera images and maps.

The problem of localizing a robot on a 2-D map has been successfully tackled by particle filter methods, i.e., Monte-Carlo localization [2]. Most works assume a laser rangefinder mounted on the robot, for which simple analytic observation models have been developed [31]. There has been attempts to incorporate monocular or depth cameras [32, 33, 34, 35], but obtaining a probabilistic observation model for particle filtering remains a challenge. PF-net encodes both the probabilistic models and the particle filter algorithm in a single neural network, thus allowing to learn localization end-to-end, from camera images and a map, to state estimates. We do not require direct supervision on the models, but instead expect effective models to emerge through end-to-end training.

### 3 Particle Filter Networks

We introduce the Particle Filter Network (PF-net) that encodes learnable transition and observation models, together with the particle filter algorithm, in a single neural network (Fig. 2). The unified network representation of the model and the algorithm is achieved by noticing the equivalence of neural networks and *differentiable programs*, i.e., computational graphs. With this unified representation we can combine the strength of deep learning and algorithmic reasoning. Deep neural networks can represent complex probabilistic models and deal with rich, visual input. Encoding the algorithm in the same network provides a *prior* for learning state estimation. Compared to generic architectures, such as LSTM [36], PF-net encodes structure specific to sequential probabilistic estimation: it uses the particle representation of probability distributions, and Bayesian updates for transitions and observations. Compared to conventional model-based methods, PF-net learns a model end-to-end, i.e., it optimizes the model for the task objective in the context of an algorithm. End-to-end PF-net may not need to learn the entire conditional distribution in its probabilistic model; instead, it may learn only the relevant features for state estimation. In this section we provide background on particle filtering and introduce the general PF-net architecture. In Sect. 4 we apply PF-net to visual localization.

#### 3.1 Particle filter algorithm

Particle filters periodically approximate the posterior distribution over states after an observation is received, i.e., they maintain a belief over states,  $b(s)$ . The belief is approximated by a set of *particles*, i.e., weighted samples from the probability distribution,

$$b_t(s) \approx \langle s_t^k, w_t^k \rangle_{k=1:K}, \quad (1)$$

where  $\sum_k w_k = 1$ ,  $K$  is the number of particles,  $s_k$  is the particle state,  $w_k$  is the particle weight, and  $t$  denotes time. Importantly, the particle set can approximate arbitrary distributions, e.g., continuous, multimodal, non-Gaussian distributions. The state estimate can be computed by the weighted mean,

$$\bar{s}_t = \sum_k w_t^k s_t^k. \quad (2)$$

The particles are periodically updated in a Bayesian manner. First, the particle states are updated by sampling from a probabilistic transition model,

$$s_t^k \sim T(s_t | u_t, s_{t-1}^k), \quad (3)$$

where the transition model,  $T$ , defines the probability of a state,  $s_t$ , given a previous state,  $s_{t-1}^k$ , and the last action,  $u_t$ , or odometry reading in case of robot localization. Second, the particle weights are updated. We compute the likelihood,  $f_t^k$ , for each particle,

$$f_t^k = Z(o_t | s_t^k; \mathbb{M}), \quad (4)$$

where the observation model,  $Z$ , defines the conditional probability of an observation,  $o_t$ , given a state and the 2-D floor map,  $\mathbb{M}$ . Particle weights are updated according to the likelihoods,

$$w_t^k = \eta f_t^k w_{t-1}^k, \quad (5)$$

where  $\eta^{-1} = \sum_{j \in K} f_t^j w_{t-1}^j$  is a normalization factor.

One common issue is particle degeneracy, i.e., when only few particles have non-zero weight. The problem is typically addressed by *resampling*. We sample a new set of particles from the current set with repetition, where a particle is chosen with a probability proportionate to its weight,

$$p(k) = w_t^k. \quad (6)$$

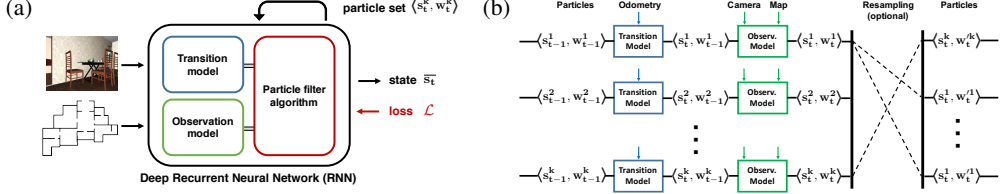


Figure 2: (a) PF-net encodes the transition and observations models together with the particle filter algorithm in a single RNN. (b) Particle update in the PF-net computational graph. The transition and observation models can be learnable neural networks, with their weights shared across particles.

The weights are then updated according to a uniform distribution,

$$w_t'^k = 1/K. \quad (7)$$

The new particle set approximates the same distribution, but devotes its representation power to the important regions of the space. The new set may contain repeated particles, but these will diverge later because of stochastic transition updates.

### 3.2 PF-net architecture

PF-net encodes the particle filter algorithm in an RNN, together with the probabilistic transition and observation models. The key idea for this unified representation is to view neural networks as differentiable programs, or computation graphs. PF-net implements the algorithmic steps of particle filtering (1)-(5) as a differentiable program, where differentiable operations are applied on tensors in a computational graph. See Fig. 2a for the PF-net architecture and Fig. 2b for the computational graph of an update step. From the neural network perspective PF-net is an RNN, where the hidden state corresponds to the particle set defined in (1). The transition and observation models, (3) and (4), are represented by neural networks with appropriate structure and, optionally, learnable parameters. In contrast to the model, we do not learn the algorithm. Rather, we use the algorithm as inductive bias, i.e., *a prior* on the network architecture.

We need all operations to be differentiable in a differentiable program, so that we can train the learnable neural network components using backpropagation. In particle filters the only non-differentiable operations are sampling from a learned distribution in (3), and resampling particles in (6)-(7). The former can be turned into a differentiable operation using the “reparameterization trick” introduced for Variational Autoencoders [37, 38]. The “trick” is to take a noise vector as input, and express the desired distribution as a deterministic, differentiable function of this input. The function can have learnable parameters, e.g., the mean and variance of a Gaussian.

The problem with particle resampling is that new particle weights are set to constant in (6), which then produces zero gradients. We address the problem by introducing *soft-resampling*, a differentiable approximation based on importance sampling. Instead of sampling particles from the desired  $p(k)$ , we now sample from  $q(k)$ , a combination of  $p(k)$  and a uniform distribution,

$$q(k) = \alpha w_t^k + (1 - \alpha)1/K, \quad (8)$$

where  $\alpha$  is a trade-off parameter. The new weights are then computed by the importance sampling formula,

$$w_t'^k = w_t^k q(k)^{-1}, \quad (9)$$

which has a non-zero gradient when  $\alpha \neq 1$ . Soft-resampling trades off the desired sampling distribution ( $\alpha = 1$ ) with the uniform sampling distribution ( $\alpha = 0$ ), maintaining the dependency on previous particle weights, and thus providing non-zero gradients for training.

Now we have all operations of particle filtering implemented in a differentiable manner. When applying PF-net to a particular task we must choose the representation of states, the network architecture for  $T$  and  $Z$ , and the number of particles,  $K$ . Note that we may choose different  $K$  settings for training and evaluation.

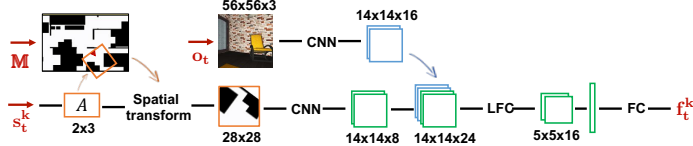


Figure 3: PF-net observation model that matches features from camera images with a 2-D map. Inputs are floor map  $\mathbb{M}$ , observation  $o_t$ , and particle state  $s_t^k$ ; output is the particle likelihood  $f_t^k$ . CNN, LFC and FC are convolutional, locally-fully-connected, and fully connected components, respectively.

## 4 Visual localization with PF-net

A robot navigates in an indoor environment it has not seen before. The robot is uncertain of its location. It has an onboard camera and odometry sensors. The task is to periodically estimate the location from the history of past sensor observations given a 2-D floor map encoding the building geometry. Formally, we seek to minimize the mean squared error over the trajectory,

$$\mathcal{L} = \sum_t (\bar{x}_t - x_t^*)^2 + (\bar{y}_t - y_t^*)^2 + \beta(\bar{\phi}_t - \phi_t^*)^2, \quad (10)$$

where  $\bar{x}_t, \bar{y}_t, \bar{\phi}_t$  and  $x_t^*, y_t^*, \phi_t^*$  are the estimated and true robot pose for time  $t$ , respectively;  $\beta$  is a constant parameter. Challenges are twofold. First, we must periodically update a posterior over states given ambiguous observations, where the posterior is a multimodal, non-Gaussian, continuous distribution. Second, we need to obtain the conditional probability of camera images given a state and a map. This involves extracting and comparing the building geometry from the schematic 2-D map and a camera image capturing a rich 3-D scene with objects, e.g. furniture, not on the map. We apply PF-net to visual localization. PF-net addresses both challenges. It encodes the structure of particle filtering for estimating arbitrary probability distributions, and it represents the observation model, and the algorithm, by a single neural network, which allows learning appropriate features for the observation model end-to-end from data.

The inputs to PF-net are the map and sensor readings from a camera and odometry. The output is the 2-D pose,  $\bar{s} = \{\bar{x}, \bar{y}, \bar{\phi}\}$ , where  $\bar{x}$  and  $\bar{y}$  are continuous coordinates, and  $\bar{\phi}$  is the continuous orientation. For end-to-end training we use the loss,  $\mathcal{L}$ . The particles in PF-net are pairs of a candidate pose,  $s_t^k$  and the corresponding weight,  $w_t^k$ . We used  $K = 30$  particles for training, and increased  $K$  up to 3000 for evaluation. In the context of RNNs, the particles can be seen as the hidden state.

The transition and observation models,  $T$  and  $Z$ , are neural network components in the PF-net. The transition model updates the particle state given the odometry input,  $u_t$ , i.e., the relative motion defined in the robot coordinate frame. Our neural network transforms  $u_t$  to the global coordinate frame,  $u'_t$ , and adds it to the previous pose along with Gaussian noise. Formally, we sample the new particle state from the differentiable function

$$T(s_t^k | u'_t, s_{t-1}^k) = s_{t-1}^k + u'_t + \text{diag}(\sigma_t, \sigma_t, \sigma_r) \mathcal{N}(0; I), \quad (11)$$

where  $\mathcal{N}(0; I)$  is noise input from a standard multivariate Gaussian;  $\sigma_t$  and  $\sigma_r$  are standard deviations for translation and rotation, respectively. In preliminary experiments we manually set  $\sigma_t$  and  $\sigma_r$ , but we could learn them from data in the future, optimizing together with the observation model.

The observation model defines the probability of a camera observation,  $o_t$ , conditioned on the particle state,  $s_t^k$ , and the floor map,  $\mathbb{M}$ . The challenge is the conditional distribution of images, that show environments with different layouts, different furniture in different configurations, etc. Instead of learning the entire conditional distribution, we learn the particle likelihoods directly. Because of training the entire network end-to-end, we only need to learn the features relevant to localization.

We propose the network shown in Fig. 3. First, a *local map* is obtained from  $\mathbb{M}$  and  $s_t^k$  through affine image transformation. For a differentiable network implementation we adopt the Spatial Transformer Network [39]. An affine transformation matrix,  $A^k$ , is computed for each particle such that the transformed image is a local view from the pose,  $s_t^k$ . Next, we extract features from the local map and the camera image through separate learned CNN components. The feature maps are concatenated, fed to a locally fully connected layer, reshaped to a vector, and fed to a final fully connected layer. The network applies to any map size. The output is a scalar,  $f_t^k$ , the likelihood of the particle state.



Figure 4: House3D data. Example for a map and RGB images from the training (top) and test (bottom) environments.

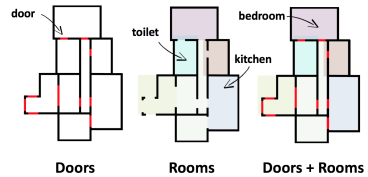


Figure 5: Semantic maps with channels for doors and rooms.

Likelihoods are obtained for each particle, and the particle weights are updated using (5). Note that observation features only need to be computed once, and learned network weights are shared across particles. Finally, we normalize the particle weights and resample particles using (8)-(9). Because of the low uncertainty setting in our experiments, during training we simply carried over particles to the next step, and only used resampling during evaluation. Resampling during training can be important for high uncertainties, or for jointly optimizing transition and observation models.

## 5 Experiments

We evaluated PF-net in simulation experiments, where it successfully learned to localize in previously unseen, realistic environments with furniture, which is not on the map. We considered multiple variants of the task: tracking (low uncertainty) and global localization (high uncertainty); laser, depth and monocular camera sensors; and floor maps with semantic labels for doors and rooms. PF-net outperformed alternative architectures in all settings, because of its suitable algorithmic prior for sequential state estimation. Compared to a conventional model-based method, i.e., the beam laser model, PF-net learned more effective models end-to-end. Results are summarized in Table 1.

### 5.1 Experimental setup

**Simulation data.** We conducted experiments in the House3D simulator [22] which builds on a large set of human-designed, realistic residential buildings from the SUNCG dataset [40]. We used 45k trajectories from 200 buildings for training, and 820 trajectories from a separate set of 47 buildings for evaluation. See Fig. 4 for examples. The trajectories are generated at random. The robot moves forward ( $p=0.8$ ) or turns ( $p=0.8$ ). The distance and turning angles are sampled uniform from [20cm, 80cm] and [15°, 60°]. The average room size is 37m<sup>2</sup>, the average building size is 206m<sup>2</sup>.

**Tracking and global localization.** We tried localization with low and high initial state uncertainty. The former is called *tracking*, and the latter is called *global localization*. The initial belief for tracking is a multivariate Gaussian with  $\Sigma = \text{diag}(30\text{cm}, 30\text{cm}, 30^\circ)$ , where the center is offset randomly, sampled from the same Gaussian. The initial belief for global localization is uniform over states in an area, including orientations. We tried initial beliefs of increasing difficulty: room-level, i.e., uniform over one room; uniform over two rooms; and uniform over all rooms, i.e., the entire building.

**Sensors, semantic maps and furniture.** While our motivation is localizing with a monocular camera (RGB images), we also tried PF-net with laser and depth sensors. We simulated the laser sensor by a virtual rangefinder, i.e., depth images transformed to 1-D laser-scans. Compared to a typical laser sensor, localization with the virtual rangefinder is harder, because of the narrow field of view of the camera. To explore if PF-net can learn simple sensor fusion, we combined depth and RGB inputs, i.e., we created RGB-D images. We also explored if PF-net can learn to use simple semantic maps, i.e., which indicate doors and room categories as in Fig. 5. We encoded the semantic labels in separate channels of the input map: one channel for doors, 8 channels for 8 distinct room categories. The PF-net architecture was the same for all variants of the localization task, only the input shape varied. Finally, to understand the effect of objects not on the map, e.g., furniture, we included simplified environments with only walls, no furniture. These are indicated by (*walls*) in Table 1.

**Implementation, training and evaluation.** We implemented PF-net in Tensorflow [41]. We trained by backpropagation through time, limited to 4 time steps. We used the RMSProp optimizer [42] with the end-to-end loss from (10). All networks, PF-net and its alternatives, were trained for tracking on 24-step long trajectories. We then evaluated learned models for both tracking and global localization, on 24 and 100 step trajectories, respectively.

	RGB	Depth	RGB Depth	Laser	Laser (walls)
Baseline	109.4	109.4	109.4	109.4	109.4
HF network	92.0	91.6	89.8	95.6	92.4
LSTM network	66.9	58.8	60.3	74.2	64.4
PF (beam model)	—	—	—	81.3	<b>31.3</b>
<b>PF-net (ours)</b>	<b>40.5</b>	<b>35.9</b>	<b>33.3</b>	<b>48.3</b>	31.5

(a) Tracking. RMSE in cm (lower is better).

	RGB	Depth	RGB Depth
—	82.6%	84.0%	84.3%
Doors	84.4%	83.9%	84.5%
Rooms	84.5%	86.2%	86.5%
Both	<b>84.6%</b>	<b>86.7%</b>	<b>87.2%</b>

(c) Semantic map variants (rows). Global localization, PF-net.

	RGB	Depth	RGB Depth	Laser	Laser (walls)
Baseline	1.1%	1.1%	1.1%	1.1%	1.1%
HF network	2.7%	2.9%	4.5%	1.6%	2.2%
LSTM network	21.1%	24.4%	23.4%	17.2%	22.2%
PF (beam model)	—	—	—	25.1%	86.2%
<b>PF-net (ours)</b>	<b>82.6%</b>	<b>84.0%</b>	<b>84.3%</b>	<b>69.4%</b>	<b>86.6%</b>

(b) Localization, room-level. Success rate (higher is better).

K	Initial belief # rooms		
	one	two	all
500	80.0%	70.5%	46.1%
1,000	84.3%	80.1%	57.9%
2,000	87.3%	84.8%	68.5%
3,000	<b>89.0%</b>	<b>85.9%</b>	<b>76.3%</b>

(d) Global localization, PF-net. Initial belief vs. particle count,  $K$ .

Table 1: Main results, averaged over test trajectories. We used  $K = 300$  particles for tracking, and  $K = 1000$  for localization, for both PF and PF-net. (a) Tracking. Compares PF-net and alternatives for different sensor inputs. (b) Localization. Success rates with room-level initial belief. (c) Localization with semantic maps. Success rates for PF-net, room-level initial belief. Rows are for different semantic labels on the map. (d) Global localization. Success rate for PF-net with RGB + depth input. Rows are for different  $K$  settings. Columns are for initial belief uniform over one, two, and all rooms.

## 5.2 Results and discussion

Main results are summarized in Table 1. An example for successful localization is shown in Fig. 6. For tracking we report the Root Mean Squared Error (RMSE) in cm, computed for the  $x, y$  components. For global localization we report success rate in percentage. Localization is successful if the estimation error is below 1m for the last 25 steps of the 100-step long trajectory. Results are averaged over a fixed set of 820 random trajectories in 47, previously unseen environments. For reference we provide the propagated uncertainty, *baseline* in Table 1. The propagated uncertainty is the performance when transition updates are performed on the initial belief, but not the observation updates, thus the uncertainty increases, but it is never reduced. We compare PF-net to alternative network learning architectures, Histogram filter network, *HF network*, and LSTM network; as well as a model-based approach, particle filtering with the beam laser model, *PF (beam model)*.

**PF-nets successfully localize in new environments with furniture.** PF-net successfully learned to localize on a 2-D map in previously unseen environments, populated with objects, e.g., furniture, that are not on the map. Learned PF-nets reduce state uncertainty in the tracking setting (Table 1a), and successfully localize with room-level uncertainty in the global localization setting (Table 1b–c). By increasing the number of particles, PF-nets can localize even when entirely lost in large environments (Table 1d). PF-net can deal with arbitrary, multimodal beliefs, because of the powerful particle representation. See Fig. 6 for an example. PF-net is effective with various sensors, including the rich, thus challenging, RGB images. Learned RGB models in fact preform better than laser models; and they are not far behind depth models. End-to-end PF-nets provide an opportunity for simple sensor fusion: when we combine RGB and depth inputs, performance improves (*RGB Depth* in Table 1), which indicates potential for future work in this direction.

**Algorithmic priors are useful.** The algorithmic priors in PF-net, i.e., the particle representation of beliefs and their Bayesian update, are beneficial for sequential state estimation. PF-net consistently outperformed alternative end-to-end learning architectures with weaker priors: Histogram filter network [16], and LSTM network [36]. Histogram filter network represents the belief by a histogram, i.e., a table of probability values, and thus it does not scale well to a large or continuous state space. For visual input we used a network architecture similar to PF-net. The state space was discretized to 16 orientations and a grid of the size of the input map, scaled down by a factor of 20. We could not achieve better results with finer discretization. The LSTM network is not restricted to a discrete

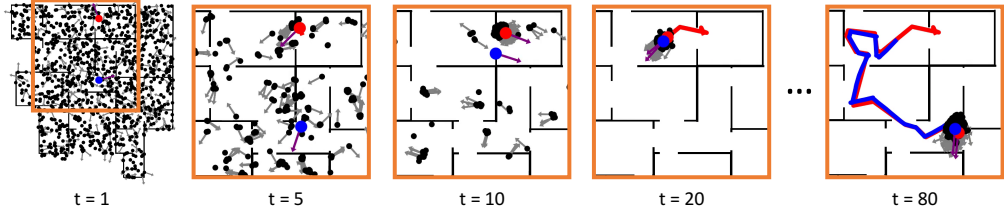


Figure 6: Successful global localization with PF-net, RGB input,  $K = 1000$ . Red indicates ground-truth, blue indicates PF-net estimate, black indicates PF-net particles.

grid, but it has no structure specific to probabilistic state estimation, i.e., it must rely on its hidden state to represent a belief. We used a network architecture similar to the observation model in PF-net, extended by an LSTM layer. The network receives an image and a local map, and outputs a relative state estimate. The relative state is added to the previous state, and the map is transformed to the local view from the updated state. We also tried alternative, vanilla LSTM architectures that directly map from global map, observation and current state to next state, but the performance was much worse.

**We can learn better models end-to-end.** We compared learned PF-nets to particle filtering with a fixed laser beam model, a standard approach to robot localization with laser sensors [31]. In particular, we used the beam model implementation in the AMCL package of ROS [43], and tuned the model parameters for our virtual laser sensor. When only walls are rendered in the environment, the performance is similar (*Laser (walls)* column in Table 1a–b). When the environment is populated with objects (*Laser* column), learned PF-net models perform significantly better. Why? The beam model decouples the laser-scan to individual laser beams, and thus it has no principled way to distinguish relevant walls, from irrelevant objects. In contrast, PF-net processes the laser-scan jointly, and may learn relationship between laser-beams to distinguish walls from objects. In addition, PF-net can learn to deal with imperfect maps, e.g., missing walls, glass doors, and artifacts at the edge of the map, which we all observed occasionally in the House3D dataset.

**Semantic maps.** Unlike typical robot localization methods, humans use floor maps with semantic information, e.g., labels for the office, kitchen, toilet, as well as lifts and staircases. However, utilizing semantic maps in models for robot localization is not trivial [35, 44]. PF-net provides an opportunity for learning this end-to-end. Preliminary results (Table 1c) show that simple semantic maps, which indicate doors or room labels, can indeed improve localization performance.

**Towards real-world localization.** Future work may extend our experiments with PF-nets to real-world localization, a problem of great interest for mobile robot applications. One concern is online execution. With RGB input PF-net needs approx. 0.6ms per particle per step. Indoor localization with high uncertainty may require up to 1,000 – 10,000 particles [2]. We can increase robustness, and use less particles, by incorporating standard techniques for particle filtering, e.g., inserting particles or adaptive resampling [45]. We may also improve inference time, leveraging an abundance of work optimizing neural network models and hardware [46]. Finally, learned PF-net models can be used for standard particle filtering, and thus visual sensors can be complementary to laser, potentially at a lower update frequency.

## 6 Conclusion

We proposed to integrate deep learning and algorithmic reasoning for probabilistic state estimation. We introduced PF-net that encodes learned probabilistic models, together with the particle filter algorithm, in a unified neural network architecture. We applied PF-net to map-based localization, and introduced a suitable network architecture for matching features from rich visual sensory input and a crude 2-D map. Through end-to-end training, PF-net successfully learned to localize in challenging, previously unseen environments populated with furniture that is not on the map.

PF-net could be applied to other domains in the future, e.g., visual object tracking or SLAM, where maintaining a probabilistic belief can be crucial. An exciting line of future work may extend PF-net to learn latent state representations for filtering, potentially in an unsupervised setting. Finally, the particle representation of beliefs can be important for encoding more sophisticated algorithms in neural networks, e.g., for planning under partial observability.

## References

- [1] A. Doucet, N. De Freitas, and N. Gordon. An introduction to sequential monte carlo methods. In *Sequential Monte Carlo methods in practice*, pages 3–14. Springer, 2001.
- [2] S. Thrun, D. Fox, W. Burgard, and F. Dellaert. Robust monte carlo localization for mobile robots. *Artificial intelligence*, 128(1-2):99–141, 2001.
- [3] S. Thrun. Particle filters in robotics. In *Proceedings of the Eighteenth conference on Uncertainty in artificial intelligence*, pages 511–518. Morgan Kaufmann Publishers Inc., 2002.
- [4] M. Montemerlo, S. Thrun, D. Koller, B. Wegbreit, et al. Fastslam: A factored solution to the simultaneous localization and mapping problem. *Aaaai/iaai*, 593598, 2002.
- [5] A. Blake and M. Isard. The condensation algorithm-conditional density propagation and applications to visual tracking. In *Advances in Neural Information Processing Systems*, pages 361–367, 1997.
- [6] B. Ristic, S. Arulampalam, and N. Gordon. *Beyond the Kalman filter: Particle filters for tracking applications*. Artech house, 2003.
- [7] P. Del Moral, A. Doucet, and A. Jasra. Sequential monte carlo samplers. *Journal of the Royal Statistical Society: Series B (Statistical Methodology)*, 68(3):411–436, 2006.
- [8] J. S. Liu. *Monte Carlo strategies in scientific computing*. Springer Science & Business Media, 2008.
- [9] A. Doucet, N. De Freitas, and N. Gordon. Sequential monte carlo methods in practice. series statistics for engineering and information science, 2001.
- [10] N. Ye, A. Soman, D. Hsu, and W. S. Lee. Despot: Online POMDP planning with regularization. *Journal of Artificial Intelligence Research*, 58:231–266, 2017.
- [11] G. Shani, R. I. Brafman, and S. E. Shimony. Model-based online learning of POMDPs. In *European Conference on Machine Learning*, pages 353–364, 2005.
- [12] B. Boots, S. M. Siddiqi, and G. J. Gordon. Closing the learning-planning loop with predictive state representations. *The International Journal of Robotics Research*, 30(7):954–966, 2011.
- [13] L. Getoor, N. Friedman, D. Koller, and B. Taskar. Learning probabilistic models of link structure. *Journal of Machine Learning Research*, 3(Dec):679–707, 2002.
- [14] A. Tamar, S. Levine, P. Abbeel, Y. Wu, and G. Thomas. Value iteration networks. In *Advances in Neural Information Processing Systems*, pages 2146–2154, 2016.
- [15] T. Haarnoja, A. Ajay, S. Levine, and P. Abbeel. Backprop kf: Learning discriminative deterministic state estimators. In *Advances in Neural Information Processing Systems*, pages 4376–4384, 2016.
- [16] R. Jonschkowski and O. Brock. End-to-end learnable histogram filters. In *Workshop on Deep Learning for Action and Interaction at NIPS*, 2016.
- [17] P. Karkus, D. Hsu, and W. S. Lee. QMDP-net: Deep learning for planning under partial observability. In *Advances in Neural Information Processing Systems*, pages 4697–4707, 2017.
- [18] J. Oh, S. Singh, and H. Lee. Value prediction network. In *Advances in Neural Information Processing Systems*, pages 6120–6130, 2017.
- [19] G. Farquhar, T. Rocktäschel, M. Igl, and S. Whiteson. TreeQN and ATreeC: Differentiable tree planning for deep reinforcement learning. *arXiv preprint arXiv:1710.11417*, 2017.
- [20] B. Amos and J. Z. Kolter. Optnet: Differentiable optimization as a layer in neural networks. In *International Conference on Machine Learning*, pages 136–145, 2017.
- [21] T. Shankar, S. K. Dwivedy, and P. Guha. Reinforcement learning via recurrent convolutional neural networks. In *International Conference on Pattern Recognition*, pages 2592–2597, 2016.
- [22] Y. Wu, Y. Wu, G. Gkioxari, and Y. Tian. Building generalizable agents with a realistic and rich 3d environment. *arXiv preprint arXiv:1801.02209*, 2018.
- [23] A. Guez, T. Weber, I. Antonoglou, K. Simonyan, O. Vinyals, D. Wierstra, R. Munos, and D. Silver. Learning to search with MCTSnets. *arXiv preprint arXiv:1802.04697*, 2018.
- [24] M. Okada, L. Rigazio, and T. Aoshima. Path integral networks: End-to-end differentiable optimal control. *arXiv preprint arXiv:1706.09597*, 2017.
- [25] P. Dondi, B. Amos, and J. Z. Kolter. Task-based end-to-end model learning in stochastic optimization. In *Advances in Neural Information Processing Systems*, pages 5484–5494, 2017.

[26] R. Jonschkowski, D. Rastogi, and O. Brock. Differentiable particle filters: End-to-end learning with algorithmic priors. *arXiv preprint arXiv:1805.11122*, 2018.

[27] C. A. Naesseth, S. W. Linderman, R. Ranganath, and D. M. Blei. Variational sequential monte carlo. *arXiv preprint arXiv:1705.11140*, 2017.

[28] C. J. Maddison, J. Lawson, G. Tucker, N. Heess, M. Norouzi, A. Mnih, A. Doucet, and Y. Teh. Filtering variational objectives. In *Advances in Neural Information Processing Systems*, pages 6576–6586, 2017.

[29] T. A. Le, M. Igl, T. Rainforth, T. Jin, and F. Wood. Auto-encoding sequential monte carlo. In *Proceedings of the 6th International Conference on Learning Representations (ICLR)*, 2018.

[30] S. Gu, Z. Ghahramani, and R. E. Turner. Neural adaptive sequential monte carlo. In *Advances in Neural Information Processing Systems*, pages 2629–2637, 2015.

[31] S. Thrun, W. Burgard, and D. Fox. *Probabilistic robotics*. MIT press, 2005.

[32] F. Dellaert, W. Burgard, D. Fox, and S. Thrun. Using the condensation algorithm for robust, vision-based mobile robot localization. In *Computer Vision and Pattern Recognition, 1999. IEEE Computer Society Conference on.*, volume 2, pages 588–594. IEEE, 1999.

[33] P. Elinas and J. J. Little.  $\sigma$ mcl: Monte-carlo localization for mobile robots with stereo vision. In *Proc. of Robotics: Science and Systems (RSS)*, 2005.

[34] B. Coltin and M. Veloso. Multi-observation sensor resetting localization with ambiguous landmarks. *Autonomous Robots*, 35(2-3):221–237, 2013.

[35] O. Mendez, S. Hadfield, N. Pugeault, and R. Bowden. Sedar-semantic detection and ranging: Humans can localise without lidar, can robots? *arXiv preprint arXiv:1709.01500*, 2017.

[36] S. Hochreiter and J. Schmidhuber. Long short-term memory. *Neural Computation*, 9(8):1735–1780, 1997.

[37] D. P. Kingma and M. Welling. Auto-encoding variational bayes. *arXiv preprint arXiv:1312.6114*, 2013.

[38] C. Doersch. Tutorial on variational autoencoders. *arXiv preprint arXiv:1606.05908*, 2016.

[39] M. Jaderberg, K. Simonyan, A. Zisserman, et al. Spatial transformer networks. In *Advances in neural information processing systems*, pages 2017–2025, 2015.

[40] S. Song, F. Yu, A. Zeng, A. X. Chang, M. Savva, and T. Funkhouser. Semantic scene completion from a single depth image. In *IEEE Conference on Computer Vision and Pattern Recognition*, pages 190–198, 2017.

[41] M. Abadi, A. Agarwal, P. Barham, E. Brevdo, Z. Chen, C. Citro, G. S. Corrado, A. Davis, J. Dean, M. Devin, et al. TensorFlow: Large-scale machine learning on heterogeneous systems, 2015.

[42] T. Tieleman and G. Hinton. Lecture 6.5 - rmsprop: Divide the gradient by a running average of its recent magnitude. *COURSERA: Neural networks for machine learning*, pages 26–31, 2012.

[43] M. Quigley, K. Conley, B. Gerkey, J. Faust, T. Foote, J. Leibs, R. Wheeler, and A. Y. Ng. Ros: an open-source robot operating system. In *ICRA workshop on open source software*, 2009.

[44] O. Mozos and W. Burgard. Supervised learning of topological maps using semantic information extracted from range data. In *IEEE/RSJ International Conference on Intelligent Robots and Systems*, 2006.

[45] A. Doucet and A. M. Johansen. A tutorial on particle filtering and smoothing: Fifteen years later. *Handbook of nonlinear filtering*, 12(656-704):3, 2009.

[46] V. Sze, Y.-H. Chen, T.-J. Yang, and J. S. Emer. Efficient processing of deep neural networks: A tutorial and survey. *Proceedings of the IEEE*, 105(12):2295–2329, 2017.